Eur. Phys. J. C (2022) 82:841
https://doi.org/10.1140/epjc/s10052-022-10806-y

THE EUROPEAN PHYSICAL JOURNAL C

Regular Article - Theoretical Physics

Investigating two-zero textures of inverse neutrino mass matrix under the lamp post of LMA and LMA-D solutions and symmetry realization

Labh Singh[a], **Monal Kashav**[b], **Surender Verma**[c]

Department of Physics and Astronomical Science, Central University of Himachal Pradesh, Dharamshala 176215, India

Received: 4 May 2022 / Accepted: 14 September 2022 / Published online: 27 September 2022

Abstract In this work we have investigated the phenomenological consequences of two-zero textures of *inverse* neutrino mass matrix (M_ν^{-1}) in light of the large mixing angle (LMA) and large mixing angle-*dark* (LMA-D) solutions, later of which originates if neutrinos exhibit non-standard interactions with matter. Out of fifteen possibilities, only seven two-zero textures of M_ν^{-1} are found to be phenomenologically allowed under LMA and/or LMA-D descriptions. In particular, five textures are in consonance with both LMA and LMA-D solutions and are necessarily CP violating while remaining two textures are found to be consistent with LMA solution only. The textures with vanishing (1, 1) element of M_ν^{-1} are, in general, disallowed. All the textures allowed under LMA and LMA-D solutions follow the same neutrino mass hierarchy. Furthermore, textures with vanishing (2, 3) element of M_ν^{-1} are found to be either disallowed or are consistent with LMA description only. We have, also, obtained the implication of the model for $0\nu\beta\beta$ decay amplitude $|M_{ee}|$. For most of the textures the calculated 3σ lower bound on $|M_{ee}|$ is $\mathcal{O}(10^{-2})$, which is within the sensitivity reach of $0\nu\beta\beta$ decay experiments. We have, also, proposed a flavor model based on discrete non-Abelian flavor group A_4 wherein such textures of M_ν^{-1} can be realized within Type-I seesaw setting.

1 Introduction

The experimental evidences accumulated in last two decades have convincingly established that not only neutrino have non-zero mass but its dynamical origin is beyond our current understanding of the standard model (SM). Despite the best efforts to precisely decipher the structure of neutrino mixing matrix, it still has certain unknowns, for example, CP violating phases, octant of θ_{23} and neutrino mass hierarchy, to name a few. The theoretical frameworks to explain neutrino mass and its manifestations like neutrino oscillations have been developed assuming standard [charged (CC) and neutral current (NC)] interactions between neutrino and matter. These frameworks culminated in large mixing angle (LMA) solution to the solar neutrino problem (SNP) and is well established by the neutrino oscillation experiments. In fact LMA has been independently confirmed as the solution to solar neutrino problem (SNP) in solar and KamLAND reactor experiments [1]. It has been shown that for positive solar mass-squared difference, $\sin^2\theta_{12}$ cannot be greater than 0.5. However, at the subdominant level, there still have possibilities for additional contributions to neutrino oscillations such as non-standard interactions (NSI) of neutrino with matter fields [2–4]. The future hyper-technological experiments will have the access to these unexplored regions. In presence of NSI, θ_{12} can be in the second octant. Thus, solar neutrino problem may have another degenerate solution in which $\sin^2\theta_{12} \approx 0.7$. This solution is termed as large mixing angle-*dark* (LMA-D) solution. In general, the degeneracy between LMA and LMA-D solutions cannot be alleviated by oscillation experiments due to generalized mass hierarchy degeneracy in presence of NSI. However, a combined measurements from neutrino oscillation and scattering experiments may have imperative implication with regard to lifting of these degeneracies [5–7]. Although non-standard interactions of neutrino with matter are severely constrained, the latest global fit, incorporating neutrino oscillation and COHERENT data, still allows LMA-D solution at 3σ confidence level [8]. The only difference in LMA and LMA-D is in

[a] e-mail: sainilabh5@gmail.com
[b] e-mail: monalkashav@gmail.com
[c] e-mail: s_7verma@yahoo.co.in (corresponding author)

the octant of θ_{12}, however, the solar mass-squared difference remains the same.

The progress in understanding the origin of neutrino mass centrally involves explaining the observed pattern of neutrino mixing which is encoded in the neutrino mass matrix obtained after electroweak symmetry breaking. Assuming neutrino to be Majorana particle the mass matrix contain nine free parameters *viz.* three neutrino mass eigenvalues, three mixing angles and three CP violating phases. The two mass-squared differences and three mixing angles have been measured in neutrino oscillation experiments with high degree of precision. Seesaw mechanism is a natural and most effective way to explain the smallness of neutrino mass. Within Type-I seesaw [9,10] paradigm, the low energy effective neutrino mass matrix (M_ν) is generated from Dirac neutrino mass matrix (M_D) and heavy right-handed Majorana neutrino mass matrix (M_R) using the relation: $M_\nu \approx M_D M_R^{-1} M_D^T$. The existence of near degeneracy in LMA and LMA-D solutions have imperative implications for models of neutrino mass and associated phenomenology. Recently, the LMA and LMA-D phenomenology of Majorana neutrino mass matrix has been studied assuming (i) zero textures of the neutrino mass matrix, M_ν [11–13] (ii) in presence of one-sterile neutrino [14]. Texture-zeros in the effective low energy Majorana neutrino mass matrix may have seesaw origin in which they can be realized from the zeros in M_D and M_R [15]. In literature, there have been phenomenological studies with texture one-zero [16–19] and two-zeros [20–24] while three-zeros or more, in neutrino mass matrix, are ruled out by current neutrino oscillation data [25]. In Type-I seesaw, an interesting scenario may emerge if we work in M_D-diagonal basis. In this basis, the zero(s) in M_ν^{-1} is same as the the zero(s) in M_R i.e. $M_\nu^{-1} \approx M_D^{-1} M_R M_D^{-1}$ [26]. In Ref. [13], the authors have investigated the phenomenological consequences of one-zero texture in M_ν^{-1} with in the context of trimaximal mixing. The LMA phenomenology of two-zero textures of M_ν^{-1} has been investigated in [27]. It is to be noted that the texture zeros in M_ν and M_ν^{-1} are, in general, independent and may have distinguishing phenomenology. Motivated by the capabilities of the future neutrino oscillation experiments in resolving these subdominant effects [28] and its important model building perspective, we investigate the phenomenological consequences of two-zero textures of M_ν^{-1}. Also, we have proposed a flavor model based on non-Abelian discrete group A_4 and Type-I seesaw, where such zeros can be realized in the inverse neutrino mass matrix. There are fifteen possibilities to have two zeros in M_ν^{-1}. We investigate the LMA and LMA-D phenomenology of these fifteen textures.

The paper is organized as follows. In Sect. 2, we briefly introduce the formalism of two-zero texture of M_ν^{-1} and the details of the numerical analysis. Section 3 is devoted to the investigation and discussion of LMA/LMA-D phenomenology of the seven allowed textures of M_ν^{-1}. A flavor model based on non-Abelian A_4 symmetry is discussed in Sect. 4. Finally, we brief our conclusions in Sect. 5.

2 Formalism of two-zero textures of inverse neutrino mass matrix

In charged lepton basis, the neutrino mass matrix is given by

$$M_\nu = V M_\nu^{diag} V^T, \tag{1}$$

where $M_\nu^{diag} = diag(m_1, m_2, m_3)$ is the neutrino mass eigenvalue matrix, $V = U.P$ is complex unitary neutrino mixing matrix. The matrix U is Pontecorvo–Maki–Nakagawa–Sakata (PMNS) matrix which in the PDG representation can be written as [29]

$$U = \begin{pmatrix} U_{11} & U_{12} & U_{13} \\ U_{21} & U_{22} & U_{23} \\ U_{31} & U_{32} & U_{33} \end{pmatrix} = \begin{pmatrix} c_{12}c_{13} & s_{12}c_{13} & s_{13}e^{-i\delta} \\ -s_{12}c_{23} - c_{12}s_{23}s_{13}e^{i\delta} & c_{12}c_{23} - s_{12}s_{23}s_{13}e^{i\delta} & s_{23}c_{13} \\ s_{12}s_{23} - c_{12}c_{23}s_{13}e^{i\delta} & -c_{12}s_{23} - s_{12}c_{23}s_{13}e^{i\delta} & c_{23}c_{13} \end{pmatrix}, \tag{2}$$

where $c_{ij} = cos\theta_{ij}$ and $s_{ij} = sin\theta_{ij}$ and δ is Dirac-type CP violating phase. Also, P is the phase matrix given by

$$P = \begin{pmatrix} 1 & 0 & 0 \\ 0 & e^{i\alpha} & 0 \\ 0 & 0 & e^{i(\beta+\delta)} \end{pmatrix},$$

where α, β are Majorana-type CP violating phases. The inverse neutrino mass matrix can be derived from Eq. (1) as

$$M_\nu^{-1} = (V M_\nu^{diag} V^T)^{-1}. \tag{3}$$

Using Eqs. (1) and (2), six independent elements of (M_ν^{-1}) can be written as

$$\left.\begin{aligned}
(M_\nu^{-1})_{11} &= \frac{1}{m_1 m_2 m_3}\Big[c_{13}^2 e^{-2i\alpha} m_3 (c_{12}^2 e^{2i\alpha} m_2 + m_1 s_{12}^2) + e^{-2i\beta} s_{13}^2 m_1 m_2\Big],\\
(M_\nu^{-1})_{12} &= \frac{1}{m_1 m_2 m_3}\Big[e^{-i(2(\alpha+\beta)+\delta)}(c_{13} e^{2i\beta} m_1 m_3 s_{12}(c_{12}c_{23}e^{i\delta} - s_{12}s_{13}s_{23})\\
&\quad + c_{13} e^{2i\alpha} m_2(-c_{12}c_{23}e^{i(2\beta+\delta)} m_3 s_{12}) + (-c_{12}^2 e^{2i\beta} m_3 + m_1) s_{13} s_{23})\Big],\\
(M_\nu^{-1})_{13} &= \frac{1}{m_1 m_2 m_3}\Big[e^{-i(2(\alpha+\beta)+\delta)}(c_{13}c_{12}(e^{2i\alpha} m_1 m_2 - e^{2i\alpha} m_3 (c_{12}^2 e^{2i\alpha} m_2 + m_1 s_{12}^2)) s_{13}\\
&\quad - c_{12}c_{13} e^{i(2\beta+\delta)}(m_1 - e^{2i\alpha} m_2) m_3 s_{12} s_{23})\Big],\\
(M_\nu^{-1})_{22} &= \frac{1}{m_1 m_2 m_3}\Big[e^{-2i(\alpha+\delta)} m_1 m_3 (c_{12}c_{23}e^{i\delta} - s_{12}s_{13 s_{23}})^2 + m_2(c_{23}^2 m_3 s_{12}^2 + 2c_{12}c_{23} m_3 s_{12} s_{13} s_{23}\\
&\quad + e^{-2i(\beta+\delta)}(c_{13}^2 m_1 + c_{12}^2 e^{i\beta} m_3 s_{13}^2) s_{23}^2)\Big],\\
(M_\nu^{-1})_{23} &= \frac{1}{m_1 m_2 m_3}\Big[e^{-2i(\alpha+\beta)} m_1 m_3 (c_{23}s_{12}s_{13} + c_{12}e^{i\delta} s_{23})(c_{12}c_{23}e^{i\delta} - s_{12}s_{23}s_{13})\\
&\quad + e^{-2i(\beta+\delta)} m_2 (c_{23}(c_{13}^2 m_1 - e^{2i(\beta+\delta)} m_3 s_{12}^2) + c_{12}^2 c_{23} e^{i\beta} m_3 s_{13}^2 s_{23}\\
&\quad + c_{12} e^{i(2\beta+\delta)} m_3 s_{12} s_{23}(c_{23}^2 - s_{23}^2))\Big],\\
(M_\nu^{-1})_{33} &= \frac{1}{m_1 m_2 m_3}\Big[e^{-2i(\alpha+\beta+\delta)} c_{23}^2 (c_{13}^2 e^{2i\alpha} m_1 m_2 + e^{2i\beta} m_3 (c_{12}^2 e^{2i\alpha} m_2 + m_1 s_{12}^2) s_{13}^2)\\
&\quad + e^{i(2\alpha+\delta)} 2c_{12}c_{23}(m_1 - e^{2i\alpha} m_2) m_3 s_{12} s_{13} s_{23} + e^{-2i\alpha} m_3 (c_{12}^2 m_1 + e^{2i\alpha} m_2 s_{12}^2) s_{23}^2\Big].
\end{aligned}\right\} \tag{4}$$

There are fifteen possible two-zero textures of M_ν^{-1} which we categorize in five classes *viz.* class A, B, C, D and E as shown in Table 1. Symbolically, these 15 textures can be represented as

$$A_1 = \begin{pmatrix} 0 & 0 & X \\ 0 & X & X \\ X & X & X \end{pmatrix}, A_2 = \begin{pmatrix} 0 & X & 0 \\ X & X & X \\ 0 & X & X \end{pmatrix}, A_3 = \begin{pmatrix} 0 & X & X \\ X & 0 & X \\ X & X & X \end{pmatrix},$$

$$A_4 = \begin{pmatrix} 0 & X & X \\ X & X & 0 \\ X & 0 & X \end{pmatrix}, A_5 = \begin{pmatrix} 0 & X & X \\ X & X & X \\ X & X & 0 \end{pmatrix};$$

$$B_1 = \begin{pmatrix} X & 0 & 0 \\ 0 & X & X \\ 0 & X & X \end{pmatrix}, B_2 = \begin{pmatrix} X & 0 & X \\ 0 & 0 & X \\ X & X & X \end{pmatrix}, B_3 = \begin{pmatrix} X & 0 & X \\ 0 & X & 0 \\ X & 0 & X \end{pmatrix},$$

$$B_4 = \begin{pmatrix} X & 0 & X \\ 0 & X & X \\ X & X & 0 \end{pmatrix};$$

$$C_1 = \begin{pmatrix} X & X & 0 \\ X & 0 & X \\ 0 & X & X \end{pmatrix}, C_2 = \begin{pmatrix} X & X & 0 \\ X & X & 0 \\ 0 & 0 & X \end{pmatrix}, C_3 = \begin{pmatrix} X & X & 0 \\ X & X & X \\ 0 & X & 0 \end{pmatrix};$$

$$D_1 = \begin{pmatrix} X & X & X \\ X & 0 & 0 \\ X & 0 & X \end{pmatrix}, D_2 = \begin{pmatrix} X & X & X \\ X & 0 & X \\ X & X & 0 \end{pmatrix};$$

$$E_1 = \begin{pmatrix} X & X & X \\ X & X & 0 \\ X & 0 & 0 \end{pmatrix},$$

where "X" denotes the non-zero element of inverse neutrino mass matrix. In the present work, we investigate the phenomenological consequences of these 15 possible two-zero textures in M_ν^{-1} within the paradigm of LMA and LMA-D descriptions of neutrino oscillation phenomenon.

In general, two-zero texture of M_ν^{-1} result in constraining equations

$$(M_\nu^{-1})_{pq} = 0; \quad (M_\nu^{-1})_{rs} = 0 \tag{5}$$

where p, q, r and s can take value 1, 2, 3 such that $p \le q$, $r \le s$.

Using Eq. (3), the constraints described by Eq. (5) can be written as

$$\lambda_1 U^{-1}{}_{1p} U^{-1}{}_{1q} + \lambda_2 U^{-1}{}_{2p} U^{-1}{}_{2q} + \lambda_3 U^{-1}{}_{3p} U^{-1}{}_{3q} = 0, \tag{6}$$

and

$$\lambda_1 U^{-1}{}_{1r} U^{-1}{}_{1s} + \lambda_2 U^{-1}{}_{2r} U^{-1}{}_{2s} + \lambda_3 U^{-1}{}_{3r} U^{-1}{}_{3s} = 0, \tag{7}$$

Table 1 Fifteen possible two-zero texture patterns with corresponding first and second zero

Class	Textures	$(M_\nu^{-1})_{pq}=0$	$(M_\nu^{-1})_{rs}=0$
A	A_1	$(M_\nu^{-1})_{11}$	$(M_\nu^{-1})_{12}$
	A_2	$(M_\nu^{-1})_{11}$	$(M_\nu^{-1})_{13}$
	A_3	$(M_\nu^{-1})_{11}$	$(M_\nu^{-1})_{22}$
	A_4	$(M_\nu^{-1})_{11}$	$(M_\nu^{-1})_{23}$
	A_5	$(M_\nu^{-1})_{11}$	$(M_\nu^{-1})_{33}$
B	B_1	$(M_\nu^{-1})_{12}$	$(M_\nu^{-1})_{13}$
	B_2	$(M_\nu^{-1})_{12}$	$(M_\nu^{-1})_{22}$
	B_3	$(M_\nu^{-1})_{12}$	$(M_\nu^{-1})_{23}$
	B_4	$(M_\nu^{-1})_{12}$	$(M_\nu^{-1})_{33}$
C	C_1	$(M_\nu^{-1})_{13}$	$(M_\nu^{-1})_{22}$
	C_2	$(M_\nu^{-1})_{13}$	$(M_\nu^{-1})_{23}$
	C_3	$(M_\nu^{-1})_{13}$	$(M_\nu^{-1})_{33}$
D	D_1	$(M_\nu^{-1})_{22}$	$(M_\nu^{-1})_{23}$
	D_2	$(M_\nu^{-1})_{22}$	$(M_\nu^{-1})_{33}$
E	E_1	$(M_\nu^{-1})_{23}$	$(M_\nu^{-1})_{33}$

where

$$\lambda_1=\frac{1}{m_1},\quad \lambda_2=\frac{e^{-2i\alpha}}{m_2},\quad \lambda_3=\frac{e^{-2i(\beta+\delta)}}{m_3}.$$

We solve Eqs. (6) and (7) for two mass ratios $\left(\frac{m_1}{m_2}e^{-2i\alpha},\quad \frac{m_1}{m_3}e^{-2i(\beta+\delta)}\right)$

$$\frac{m_1}{m_2}e^{-2i\alpha}=\frac{U^{-1}{}_{3r}U^{-1}{}_{3s}U^{-1}{}_{1p}U^{-1}{}_{1q}-U^{-1}{}_{3p}U^{-1}{}_{3q}U^{-1}{}_{1r}U^{-1}{}_{1s}}{U^{-1}{}_{3p}U^{-1}{}_{3q}U^{-1}{}_{2r}U^{-1}{}_{2s}-U^{-1}{}_{2p}U^{-1}{}_{2q}U^{-1}{}_{3r}U^{-1}{}_{3s}},\tag{8}$$

$$\frac{m_1}{m_3}e^{-2i(\beta+\delta)}=\frac{U^{-1}{}_{1r}U^{-1}{}_{1s}U^{-1}{}_{2p}U^{-1}{}_{2q}-U^{-1}{}_{1p}U^{-1}{}_{1q}U^{-1}{}_{2r}U^{-1}{}_{2s}}{U^{-1}{}_{3p}U^{-1}{}_{3q}U^{-1}{}_{2r}U^{-1}{}_{2s}-U^{-1}{}_{2p}U^{-1}{}_{2q}U^{-1}{}_{3r}U^{-1}{}_{3s}}.\tag{9}$$

The absolute values of mass ratios are given by

$$\frac{m_1}{m_2}=\left|\frac{U^{-1}{}_{3r}U^{-1}{}_{3s}U^{-1}{}_{1p}U^{-1}{}_{1q}-U^{-1}{}_{3p}U^{-1}{}_{3q}U^{-1}{}_{1r}U^{-1}{}_{1s}}{U^{-1}{}_{3p}U^{-1}{}_{3q}U^{-1}{}_{2r}U^{-1}{}_{2s}-U^{-1}{}_{2p}U^{-1}{}_{2q}U^{-1}{}_{3r}U^{-1}{}_{3s}}\right|,\tag{10}$$

$$\frac{m_1}{m_3}=\left|\frac{U^{-1}{}_{1r}U^{-1}{}_{1s}U^{-1}{}_{2p}U^{-1}{}_{2q}-U^{-1}{}_{1p}U^{-1}{}_{1q}U^{-1}{}_{2r}U^{-1}{}_{2s}}{U^{-1}{}_{3p}U^{-1}{}_{3q}U^{-1}{}_{2r}U^{-1}{}_{2s}-U^{-1}{}_{2p}U^{-1}{}_{2q}U^{-1}{}_{3r}U^{-1}{}_{3s}}\right|,\tag{11}$$

and two Majorana phases are obtained as

$$\alpha=-\frac{1}{2}Arg\left(\frac{U^{-1}{}_{3r}U^{-1}{}_{3s}U^{-1}{}_{1p}U^{-1}{}_{1q}-U^{-1}{}_{3p}U^{-1}{}_{3q}U^{-1}{}_{1r}U^{-1}{}_{1s}}{U^{-1}{}_{3p}U^{-1}{}_{3q}U^{-1}{}_{2r}U^{-1}{}_{2s}-U^{-1}{}_{2p}U^{-1}{}_{2q}U^{-1}{}_{3r}U^{-1}{}_{3s}}\right),\tag{12}$$

$$\beta=-\frac{1}{2}Arg\left(\frac{U^{-1}{}_{1r}U^{-1}{}_{1s}U^{-1}{}_{2p}U^{-1}{}_{2q}-U^{-1}{}_{1p}U^{-1}{}_{1q}U^{-1}{}_{2r}U^{-1}{}_{2s}}{U^{-1}{}_{3p}U^{-1}{}_{3q}U^{-1}{}_{2r}U^{-1}{}_{2s}-U^{-1}{}_{2p}U^{-1}{}_{2q}U^{-1}{}_{3r}U^{-1}{}_{3s}}\right)-\delta.\tag{13}$$

It is to be noted that the mass ratios $\left(\frac{m_1}{m_2}e^{-2i\alpha},\ \frac{m_1}{m_3}e^{-2i(\beta+\delta)}\right)$ are different for each texture as they depend on the position of zero in M_ν^{-1}. For example, in case of A_1 texture

$$p=1,\quad q=1,\quad r=1,\quad s=2,$$

therefore, Eqs. (8) and (9) become

$$\frac{m_1}{m_2}e^{-2i\alpha}=\frac{U^{-1}{}_{31}U^{-1}{}_{32}U^{-1}{}_{11}U^{-1}{}_{11}-U^{-1}{}_{31}U^{-1}{}_{31}U^{-1}{}_{11}U^{-1}{}_{12}}{U^{-1}{}_{31}U^{-1}{}_{31}U^{-1}{}_{21}U^{-1}{}_{22}-U^{-1}{}_{21}U^{-1}{}_{21}U^{-1}{}_{31}U^{-1}{}_{32}},$$

$$\frac{m_1}{m_3}e^{-2i(\beta+\delta)}=\frac{U^{-1}{}_{11}U^{-1}{}_{12}U^{-1}{}_{21}U^{-1}{}_{21}-U^{-1}{}_{11}U^{-1}{}_{11}U^{-1}{}_{21}U^{-1}{}_{22}}{U^{-1}{}_{31}U^{-1}{}_{31}U^{-1}{}_{21}U^{-1}{}_{22}-U^{-1}{}_{21}U^{-1}{}_{21}U^{-1}{}_{31}U^{-1}{}_{32}},$$

while for B_2 texture

$$p=1,\quad q=2,\quad r=2,\quad s=2,$$

resulting in mass ratios

$$\frac{m_1}{m_2}e^{-2i\alpha}=\frac{U^{-1}{}_{32}U^{-1}{}_{32}U^{-1}{}_{11}U^{-1}{}_{12}-U^{-1}{}_{31}U^{-1}{}_{32}U^{-1}{}_{12}U^{-1}{}_{12}}{U^{-1}{}_{31}U^{-1}{}_{32}U^{-1}{}_{22}U^{-1}{}_{22}-U^{-1}{}_{21}U^{-1}{}_{22}U^{-1}{}_{32}U^{-1}{}_{32}},$$

$$\frac{m_1}{m_3}e^{-2i(\beta+\delta)}=\frac{U^{-1}{}_{12}U^{-1}{}_{12}U^{-1}{}_{21}U^{-1}{}_{22}-U^{-1}{}_{11}U^{-1}{}_{12}U^{-1}{}_{22}U^{-1}{}_{22}}{U^{-1}{}_{31}U^{-1}{}_{32}U^{-1}{}_{22}U^{-1}{}_{22}-U^{-1}{}_{21}U^{-1}{}_{22}U^{-1}{}_{32}U^{-1}{}_{32}}.$$

We have analytically solved the mass ratios for all possible two-zero textures which are shown in the Tables 2, 3 and 4.

The two mass-squared differences $\Delta m^2_{21}=m_2^2-m_1^2$ and $\left|\Delta m^2_{32}\right|=m_3^2-m_2^2$ alongwith mass ratios $\frac{m_1}{m_2}e^{-2i\alpha}\equiv R_{12}$, $\frac{m_1}{m_3}e^{-i(2\beta+\delta)}\equiv R_{13}$ yield two values of neutrino mass m_1 given by

$$m_1^a=|R_{12}|\sqrt{\frac{\Delta m^2_{21}}{1-|R_{12}|^2}},\quad m_1^b=|R_{13}|\sqrt{\frac{\Delta m^2_{21}+|\Delta m^2_{32}|}{1-|R_{13}|^2}},\tag{14}$$

respectively. In order to ensure the consistency of the formalism the two values (m_1^a, m_1^b) must be equal which results in mass ratio parameter

$$\frac{\Delta m^2_{21}}{|\Delta m^2_{32}|}=\frac{|R_{13}|^2\left(1-|R_{12}|^2\right)}{|R_{12}|^2-|R_{13}|^2}\equiv R_\nu.\tag{15}$$

Table 2 Mass ratios for class A

Class	Texture	Mass ratios (R_{12}, R_{13})
A	A_1	$\frac{m_1}{m_2}e^{-2i\alpha} = \frac{c_{12}\left(c_{23}e^{i\delta}s_{12}s_{13} + c_{12}s_{23}\right)}{s_{12}\left(c_{12}c_{23}e^{i\delta}s_{13} - s_{12}s_{23}\right)}$
		$\frac{m_1}{m_3}e^{-i(2\beta+\delta)} = \frac{c_{12}c_{13}^2c_{23}}{s_{13}\left(-c_{12}c_{23}e^{i\delta}s_{13} + s_{12}s_{23}\right)}$
	A_2	$\frac{m_1}{m_2}e^{-2i\alpha} = -\frac{c_{12}\left(c_{12}c_{23} - e^{i\delta}s_{12}s_{13}s_{23}\right)}{s_{12}\left(c_{23}s_{12} + c_{12}e^{i\delta}s_{13}s_{23}\right)}$
		$\frac{m_1}{m_3}e^{-i(2\beta+\delta)} = \frac{c_{12}c_{13}^2s_{23}}{s_{13}\left(c_{23}s_{12} + c_{12}e^{i\delta}s_{13}s_{23}\right)}$
	A_3	$\frac{m_1}{m_2}e^{-2i\alpha} = -\frac{\left(c_{23}e^{i\delta}s_{12}s_{13} + c_{12}s_{23}\right)\left(c_{23}e^{i\delta}s_{12}s_{13} + c_{12}(s_{13}^2 - c_{13}^2)s_{23}\right)}{c_{12}^2c_{23}^2e^{2i\delta}s_{13}^2 - 2c_{12}c_{23}e^{i\delta}s_{12}s_{13}^2s_{23} + s_{12}^2(s_{13}^4 - c_{13}^4)s_{23}}$
		$\frac{m_1}{m_3}e^{-i(2\beta+\delta)} = \frac{c_{13}^2c_{23}\left(c_{23}e^{i\delta}(c_{12}^2 - s_{12}^2) - 2c_{12}s_{12}s_{13}s_{23}\right)}{-c_{12}^2c_{23}^2e^{2i\delta}s_{13}^2 + 2c_{12}c_{23}e^{i\delta}s_{12}s_{13}^2s_{23} + s_{12}^2(s_{13}^4 - c_{13}^4)s_{23}}$
	A_4	$\frac{m_1}{m_2}e^{-2i\alpha} = \frac{c_{12}^2c_{23}^2(s_{13}^4 - c_{13}^4) - 2c_{12}c_{23}e^{i\delta}s_{12}s_{13}^3s_{23} + e^{2i\delta}s_{12}^2s_{13}^2s_{23}^2}{c_{13}^2c_{23}^2s_{12}^2 - s_{13}^2\left(c_{23}s_{12}s_{13} + c_{12}e^{i\delta}s_{23}\right)^2}$
		$\frac{m_1}{m_3}e^{-i(2\beta+\delta)} = -\frac{c_{13}^2s_{23}\left(2c_{12}c_{23}s_{12}s_{13} + e^{i\delta}(c_{12}^2 - s_{12}^2)s_{23}\right)}{-c_{13}^2c_{23}^2s_{12}^2 + s_{13}^2\left(c_{23}s_{12}s_{13} + c_{12}e^{i\delta}s_{23}\right)^2}$
	A_5	$\frac{m_1}{m_2}e^{-2i\alpha} = \frac{-c_{23}e^{2i\delta}s_{12}^2s_{13}^2s_{23} + c_{12}^2c_{23}(s_{13}^4 - c_{13}^4)s_{23} + c_{12}e^{i\delta}s_{12}s_{13}^3(c_{13}^2 - s_{13}^2)}{c_{12}^2c_{23}e^{2i\delta}s_{13}^2s_{23} + c_{23}s_{12}^2(c_{13}^4 - s_{13}^4)s_{23} + c_{12}e^{i\delta}s_{12}s_{13}^3(c_{23}^2 - s_{23}^2)}$
		$\frac{m_1}{m_3}e^{-i(2\beta+\delta)} = -\frac{-c_{13}^2\left(c_{23}e^{i\alpha}(c_{12}^2 - s_{12}^2)s_{23} + c_{12}s_{12}s_{13}(c_{23}^2 - s_{23}^2)\right)}{c_{12}^2c_{23}e^{2i\delta}s_{13}^2s_{23} + c_{23}s_{12}^2(c_{13}^4 - s_{13}^4)s_{23} + c_{12}e^{i\delta}s_{12}s_{13}^3(c_{23}^2 - s_{23}^2)}$

The 3σ experimental range of parameter R_ν defined in Eq. (15) is $0.02590 < R_\nu < 0.03656$. The allowed phenomenology of the model is obtained by restricting R_ν in the 3σ experimental range. The neutrino mass eigenvalues m_2 and m_3 can be obtained using mass square differences $\left(\Delta m_{21}^2,\ \Delta m_{32}^2\right)$ as

$$\begin{aligned} m_2 &= \sqrt{m_1^2 + \Delta m_{21}^2}; \\ m_3 &= \sqrt{m_2^2 + \Delta m_{32}^2} \quad \text{for normal hierarchy (NH)} \\ &(m_1 < m_2 < m_3), \end{aligned} \tag{16}$$

and

$$\begin{aligned} m_2 &= \sqrt{m_1^2 + \Delta m_{21}^2}; \\ m_1 &= \sqrt{m_3^2 + \Delta m_{32}^2 - \Delta m_{21}^2} \quad \text{for inverted hierarchy (IH)} \\ &(m_3 < m_1 < m_2). \end{aligned} \tag{17}$$

Also, the effective Majorana mass which governs the neutrinoless double beta($0\nu\beta\beta$) decay process is given by

$$\begin{aligned} |M_{ee}| &= \left|\sum_i V_{ei}^2 m_i\right| \\ &= \left|m_1c_{12}^2c_{13}^2 + m_2s_{12}^2c_{13}^2e^{2i\alpha} + m_3s_{13}^2e^{2i\beta}\right|. \end{aligned} \tag{18}$$

The Jarlskog CP invariant is defined as [30,31]

$$J_{CP} = s_{23}c_{23}s_{12}c_{12}s_{13}c_{13}^2 \sin\delta.$$

In the numerical analysis, to study LMA phenomenology of the model, we have randomly generated the known neutrino oscillation parameters such as θ_{ij} $(i, j = 1, 2, 3; i < j)$ and Δm_{ij}^2 $(i > j)$ using Gaussian distribution within allowed experimental range shown in Table 5. However, in order to study the viability of the model under LMA-D solution, θ_{12} is randomly generated using the uniform distribution within the range (53.71°-58.37°) [32–35].

3 LMA and LMA-D phenomenology

In this section, we have investigated the phenomenology of all possible two-zero textures of M_ν^{-1} under the paradigm of LMA and LMA-D solutions to the neutrino oscillation phenomenon.

3.1 Class A

Class A is disallowed for both LMA and LMA-D solutions. As a representative case, we have discussed the viability of A_1 texture in the following.

The mass ratios $(|R_{12}|, |R_{13}|)$ for A_1 texture up-to first order in s_{13} can be written as

$$|R_{12}| \equiv \frac{m_1}{m_2} \approx \frac{c_{12}^2}{s_{12}^2} + \frac{c_{12}c_{23}\cos\delta}{s_{12}^3s_{23}}s_{13}, \tag{19}$$

Table 3 Mass ratios for class B

Class	Texture	Mass ratios (R_{12}, R_{13})
B	B_1	$\frac{m_1}{m_2}e^{-2i\alpha} = 1$ $\frac{m_1}{m_3}e^{-i(2\beta+\delta)} = 1$
	B_2	$\frac{m_1}{m_2}e^{-2i\alpha} = -\frac{\left(c_{23}e^{i\delta}s_{12}+c_{12}s_{13}s_{23}\right)\left(c_{23}e^{i\delta}s_{12}s_{13}+c_{12}s_{23}\right)}{\left(c_{12}c_{23}e^{i\delta}-s_{12}s_{23}s_{13}\right)\left(c_{12}c_{23}e^{i\delta}s_{13}-s_{12}s_{23}\right)}$ $\frac{m_1}{m_3}e^{-i(2\beta+\delta)} = \frac{c_{23}\left(c_{23}e^{i\delta}s_{12}+c_{12}s_{13}s_{23}\right)}{s_{23}\left(c_{12}c_{23}e^{i\delta}s_{13}-s_{12}s_{23}\right)}$
	B_3	$\frac{m_1}{m_2}e^{-2i\alpha} = \frac{\left(c_{23}e^{i\delta}s_{12}+c_{12}s_{13}s_{23}\right)\left(c_{12}c_{23}-e^{i\delta}s_{12}s_{13}s_{23}\right)}{\left(c_{23}s_{12}+c_{12}e^{i\delta}s_{13}s_{23}\right)\left(c_{12}c_{23}e^{i\delta}-s_{12}s_{13}s_{23}\right)}$ $\frac{m_1}{m_3}e^{-i(2\beta+\delta)} = \frac{c_{23}e^{i\delta}s_{12}+c_{12}s_{13}s_{23}}{c_{23}s_{12}+c_{12}e^{i\delta}s_{13}s_{23}}$
	B_4	$\frac{m_1}{m_2}e^{-2i\alpha} = -\frac{\left(c_{12}^2c_{23}^2s_{13}s_{23}+e^{2i\delta}s_{12}^2s_{13}s_{23}^3+c_{12}c_{23}e^{i\delta}s_{12}(c_{13}^2c_{23}^2-s_{13}^2s_{23}^2)\right)}{c_{23}^2s_{12}^2s_{13}s_{23}+c_{12}^2e^{2i\delta}s_{13}s_{23}^3-c_{12}c_{23}e^{i\delta}s_{12}(c_{13}^2c_{23}^2-s_{13}^2s_{23}^2)}$ $\frac{m_1}{m_3}e^{-i(2\beta+\delta)} = \frac{\left(c_{12}c_{23}e^{2i\delta}s_{12}s_{23}^2+e^{i\delta}(c_{12}^2-s_{12}^2)s_{13}s_{23}^3+c_{12}c_{23}s_{12}s_{13}^2(c_{23}^2+2s_{23}^2)\right)}{c_{23}^2s_{12}^2s_{13}s_{23}+c_{12}^2e^{2i\delta}s_{13}s_{23}^3-c_{12}c_{23}e^{i\delta}s_{12}(c_{13}^2c_{23}^2-s_{13}^2s_{23}^2)}$

Table 4 Mass ratios for class C, D and E

Class	Texture	Mass ratios (R_{12}, R_{13})
C	C_1	$\frac{m_1}{m_2}e^{-2i\alpha} = -\frac{\left(c_{23}^3e^{2i\delta}s_{12}^2s_{13}+c_{12}^2c_{23}s_{13}s_{23}^2+c_{12}e^{i\delta}s_{12}s_{23}(2c_{23}^2s_{13}^2-c_{13}^2s_{23}^2)\right)}{c_{12}^2c_{23}^3s_{13}e^{2i\delta}+c_{23}s_{12}^2s_{13}s_{23}^2+c_{12}e^{i\delta}s_{12}s_{23}(-2c_{23}^2s_{13}^2+c_{13}^2s_{23}^2)}$ $\frac{m_1}{m_3}e^{-i(2\beta+\delta)} = -\frac{\left(c_{23}^3e^{i\delta}(c_{12}^2-s_{12}^2)s_{13}+c_{12}c_{23}^2e^{2i\delta}s_{12}s_{23}+c_{12}s_{12}s_{13}^2s_{23}(2c_{23}^2+s_{23}^2)\right)}{c_{12}^2c_{23}^3s_{13}e^{2i\delta}+c_{23}s_{12}^2s_{13}s_{23}^2+c_{12}e^{i\delta}s_{12}s_{23}(-2c_{23}^2s_{13}^2+c_{13}^2s_{23}^2)}$
	C_2	$\frac{m_1}{m_2}e^{-2i\alpha} = \frac{\left(c_{12}c_{23}s_{13}-e^{i\delta}s_{12}s_{23}\right)\left(c_{23}e^{i\delta}s_{12}s_{13}+c_{12}s_{23}\right)}{\left(c_{23}s_{12}s_{13}+c_{12}e^{i\delta}s_{23}\right)\left(c_{12}c_{23}e^{i\delta}s_{13}-s_{12}s_{23}\right)}$ $\frac{m_1}{m_3}e^{-i(2\beta+\delta)} = -\frac{\left(-c_{12}c_{23}s_{13}+e^{i\delta}s_{12}s_{23}\right)}{c_{12}c_{23}e^{i\delta}s_{13}-s_{12}s_{23}}$
	C_3	$\frac{m_1}{m_2}e^{-2i\alpha} = \frac{\left(c_{12}c_{23}s_{13}-e^{i\delta}s_{12}s_{23}\right)\left(c_{12}c_{23}-e^{i\delta}s_{12}s_{13}s_{23}\right)}{\left(c_{23}s_{12}s_{13}+c_{12}e^{i\delta}s_{23}\right)\left(c_{23}s_{12}+c_{12}e^{i\delta}s_{13}s_{23}\right)}$ $\frac{m_1}{m_3}e^{-i(2\beta+\delta)} = \frac{s_{23}\left(c_{12}c_{23}s_{13}-e^{i\delta}s_{12}s_{23}\right)}{c_{23}\left(c_{23}s_{12}+c_{12}e^{i\delta}s_{13}s_{23}\right)}$
D	D_1	$\frac{m_1}{m_2}e^{-2i\alpha} = -\frac{s_{12}\left(c_{23}e^{i\delta}s_{12}+c_{12}s_{13}s_{23}\right)}{c_{12}\left(c_{12}c_{23}e^{i\delta}-s_{12}s_{23}s_{13}\right)}$ $\frac{m_1}{m_3}e^{-i(2\beta+\delta)} = \frac{s_{13}\left(c_{23}s_{12}+e^{-i\delta}c_{12}s_{13}s_{23}\right)}{c_{12}c_{13}^2s_{23}}$
	D_2	$\frac{m_1}{m_2}e^{-2i\alpha} = -\frac{s_{12}\left(2c_{12}c_{23}s_{13}s_{23}+e^{i\delta}s_{12}(c_{23}^2-s_{23}^2)\right)}{c_{12}\left(-2c_{23}s_{12}s_{13}s_{23}+c_{12}e^{i\delta}(c_{23}^2-s_{23}^2)\right)}$ $\frac{m_1}{m_3}e^{-i(2\beta+\delta)} = -\frac{s_{13}\left(c_{23}^2s_{13}(c_{12}^2-s_{12}^2)-2c_{12}c_{23}s_{12}s_{23}(e^{-i\delta}s_{13}^2+e^{i\delta})+s_{13}s_{23}^2(s_{12}^2-c_{12}^2)\right)}{c_{12}c_{13}^2\left(c_{12}c_{23}^2e^{i\delta}-2c_{23}s_{12}s_{13}s_{23}-c_{12}e^{i\delta}s_{23}^2\right)}$
E	E_1	$\frac{m_1}{m_2}e^{-2i\alpha} = \frac{s_{12}\left(c_{12}c_{23}s_{13}-e^{i\delta}s_{12}s_{23}\right)}{c_{12}\left(c_{23}s_{12}s_{13}+c_{12}e^{i\delta}s_{23}\right)}$ $\frac{m_1}{m_3}e^{-i(2\beta+\delta)} = \frac{s_{13}\left(-e^{-i\delta}c_{12}c_{23}s_{13}+s_{12}s_{23}\right)}{c_{12}c_{23}c_{13}^2}$

Table 5 Global fit values of neutrino oscillation parameters [36]

Parameters	Best fit $\pm 1\sigma$ range (NH)	Best fit $\pm 1\sigma$ range (IH)
$\Delta m^2_{21} [10^{-5}\ \text{eV}^2]$	$7.50^{+0.22}_{-0.20}$	$7.50^{+0.22}_{-0.20}$
$\lvert \Delta m^2_{31} \rvert [10^{-3}\ \text{eV}^2]$	$2.55^{+0.02}_{-0.03}$	$2.45^{+0.02}_{-0.03}$
θ°_{12}	34.3 ± 1.0	34.3 ± 1.0
θ°_{23}	49.26 ± 0.79	$49.46^{+0.60}_{-0.97}$
θ°_{13}	$8.53^{+0.13}_{-0.14}$	$8.53^{+0.12}_{-0.14}$

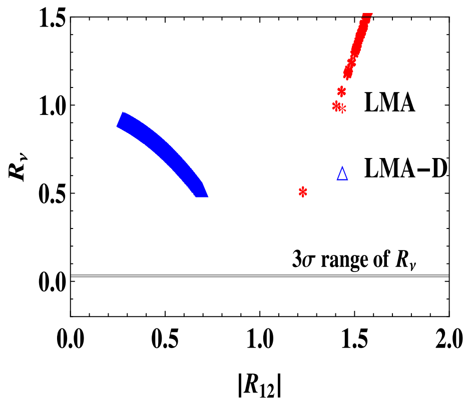

Fig. 1 Correlation between $|R_{12}|$ and R_ν for texture A_1

$$|R_{13}| \equiv \frac{m_1}{m_3} \approx \frac{c^2_{12} c^2_{23} \cos\delta}{s^2_{12} s^2_{23}} + \frac{c_{12} c_{23} \left(c^2_{12} c^2_{23} - 4 s^2_{12} s^2_{23} + 3 c^2_{12} c^2_{23} \cos 2\delta\right)}{4 s^3_{12} s^3_{23}}. \tag{20}$$

LMA Scenario: For δ in the range $0^\circ \leq \delta \leq 90^\circ$ or $270^\circ \leq \delta \leq 360^\circ$, Eq. (19) results in $\frac{m_1}{m_2} > 1$. Furthermore, if δ lie in the range $90^\circ < \delta < 270^\circ$ and $\sin\theta_{23} \approx \cos\theta_{23}$, solar mass hierarchy requires $\sin 2\theta_{12} < 4 \sin\theta_{13}$, however, from neutrino oscillation data (Table 5) $\sin 2\theta_{12} > 4 \sin\theta_{13}$ implying that A_1 texture is disallowed.

LMA-D Scenario: The parameter (R_ν) up-to first order in s_{13} can be written as

$$R_\nu \approx \left(-1 + \frac{c^4_{12}}{s^4_{12}}\right) + \frac{2 c^3_{12} c_{23} \cos\delta}{s^5_{12} s_{23}} s_{13}. \tag{21}$$

Using $\theta_{12} = 55^\circ$ and $\delta = 80^\circ$ (190°), numerical value of R_ν is found to be 0.74 (0.89) which lies outside the 3σ range of R_ν. The above observations are, also, evident from Fig. 1.

Similar analysis can be done for all remaining textures in class A. Therefore, neutrino mass model, with two-zero textures in M_ν^{-1}, wherein one of the texture zero is at (1, 1) place in M_ν^{-1} is disallowed as shown in Table 6.

3.2 Class B

In class B, mass ratios for textures B_1 are given by

$$|R_{12}| \equiv \frac{m_1}{m_2} = 1, \quad |R_{13}| \equiv \frac{m_1}{m_3} = 1,$$

Table 6 Allowed/disallowed two-zero textures of M_ν^{-1} under LMA and LMA-D solutions. The ✓ (×) mark is used to denote allowed (disallowed) texture

Class	Texture	LMA	LMA-D
A	A_1 (NH/IH)	×/×	×/×
	A_2 (NH/IH)	×/×	×/×
	A_3 (NH/IH)	×/×	×/×
	A_4 (NH/IH)	×/×	×/×
	A_5 (NH/IH)	×/×	×/×
B	B_1 (NH/IH)	×/×	×/×
	B_2 (NH/IH)	✓/×	✓/×
	B_3 (NH/IH)	×/×	×/×
	B_4 (NH/IH)	×/✓	×/✓
C	C_1 (NH/IH)	✓/×	✓/×
	C_2 (NH/IH)	×/×	×/×
	C_3 (NH/IH)	×/✓	×/✓
D	D_1 (NH/IH)	✓/×	×/×
	D_2 (NH/IH)	✓/×	✓/×
E	E_1 (NH/IH)	✓/×	×/×

Fig. 2 Correlation plots for textures B_2-NH(left panel) and B_4-IH (right panel) under LMA scenario

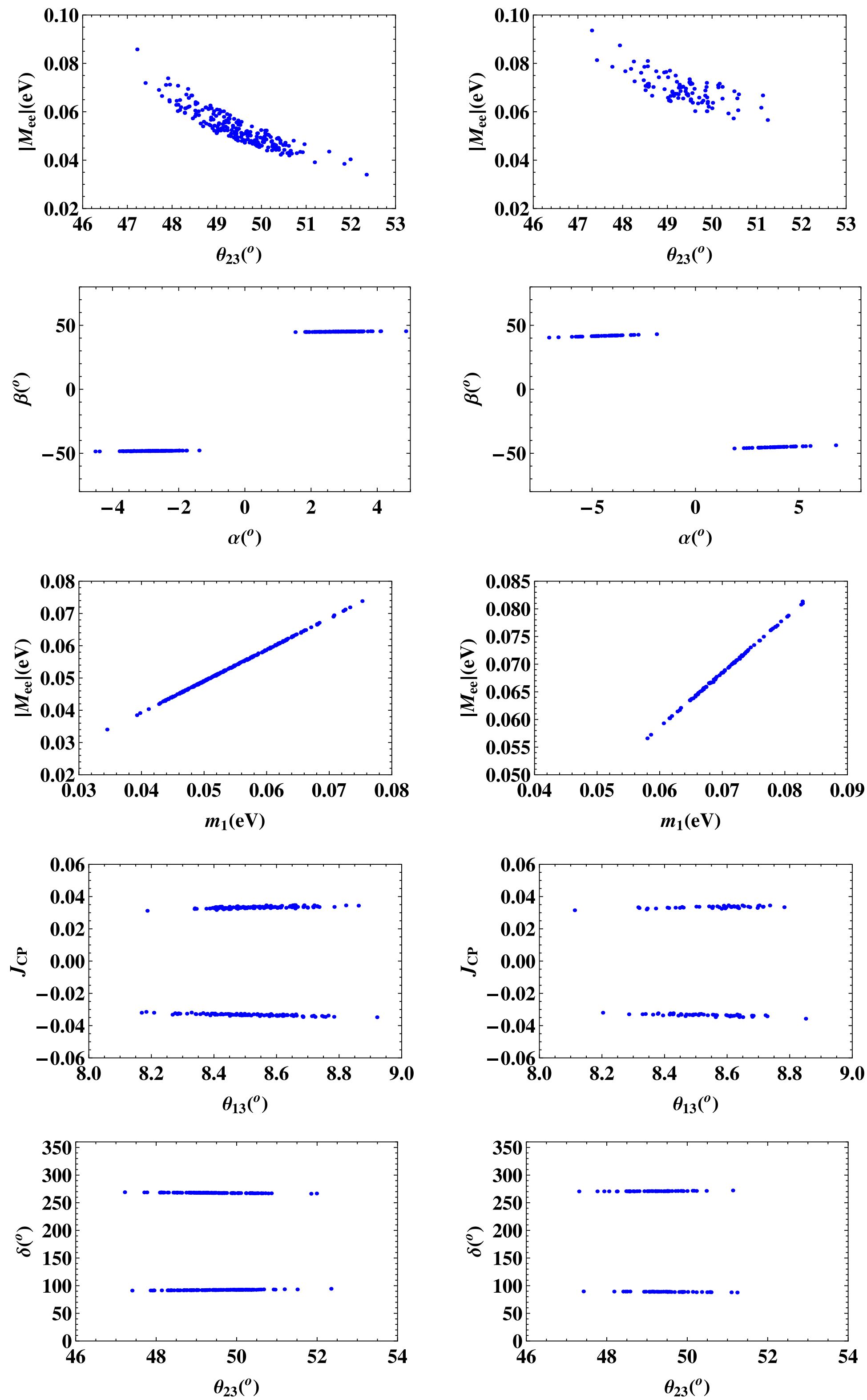

Table 7 3σ lower bound on effective Majorana mass ($|M_{ee}|$) in eV for all allowed textures. "×" symbolize the disallowed hierarchy in the corresponding texture

Allowed textures	Lower bound on $\|M_{ee}\|$ (eV)			
	LMA		LMA-D	
	NH	IH	NH	IH
B_2	0.02	×	0.04	×
B_4	×	0.06	×	0.06
C_1	0.02	×	0.02	×
C_3	×	0.06	×	0.06
D_1	0	×	×	×
D_2	0.01	×	0.02	×
E_1	0	×	×	×

which result in degenerate neutrino masses (i.e. $m_1 = m_2 = m_3$) and are inconsistent with neutrino oscillation data. Also, for texture B_3, mass ratios are given by

$$|R_{12}| = \left|\frac{\left(c_{23}e^{i\delta}s_{12} + c_{12}s_{13}s_{23}\right)\left(c_{12}c_{23} - e^{i\delta}s_{12}s_{13}s_{23}\right)}{\left(c_{23}s_{12} + c_{12}e^{i\delta}s_{13}s_{23}\right)\left(c_{12}c_{23}e^{i\delta} - s_{12}s_{13}s_{23}\right)}\right| = 1, \tag{22}$$

$$|R_{13}| = \left|\frac{c_{23}e^{i\delta}s_{12} + c_{12}s_{13}s_{23}}{c_{23}s_{12} + c_{12}e^{i\delta}s_{13}s_{23}}\right| = 1, \tag{23}$$

resulting in degenerate neutrino masses. Therefore, textures B_1 and B_3 are disallowed. In the following we have investigated the phenomenological consequences of B_2 and B_4 textures under LMA and LMA-D solutions.

The mass ratios ($|R_{12}|, |R_{13}|$) for texture B_2, up-to first order in s_{13}, can be written as

$$|R_{12}| \equiv \frac{m_1}{m_2} \approx 1 + \frac{2\cos\delta}{c_{12}c_{23}s_{12}s_{23}}s_{13}, \tag{24}$$

$$|R_{13}| \equiv \frac{m_1}{m_3} \approx \frac{c_{23}^2}{s_{23}^2} + \frac{c_{12}c_{23}\cos\delta}{s_{12}s_{23}^3}s_{13}. \tag{25}$$

From Eq. (24), in order to satisfy the solar mass hierarchy *i.e* $|R_{12}| \equiv \frac{m_1}{m_2} < 1$, δ should be in the range $90^\circ < \delta < 270^\circ$. Also, texture B_2 predicts the normal hierarchical neutrino masses for θ_{23} above maximality ($\theta_{23} > 45^\circ$) and $\cos\delta$ negative such that $|R_{13}| \equiv \dfrac{m_1}{m_3} < 1$. The above observations are, also, depicted in the Fig. 2. Similar analysis can also be done for texture B_4.

The texture B_2 (B_4) is allowed for both LMA and LMA-D solutions with normal (inverted) hierarchy. The allowed parameter space for these textures are shown in Fig. 2 as correlation plots amongst different parameters. Both these textures are found to have identical phenomenology under LMA and LMA-D solutions. In Fig. 2 we have shown the LMA scenario for B_2 (NH) and B_4 (IH) textures. In the left (right) panel we have depicted the correlation plots for B_2 (B_4) texture. The atmospheric mixing angle θ_{23} is found to be above maximality for both the textures. The CP violating phases α, β and δ are found to be sharply constrained. The Dirac-type CP violating phase δ is found to be maximal (around 90° and 270°) and the Jarlskog rephasing invariant $J_{CP} \neq 0$, thus, these textures are necessarily CP violating. We can, also, appreciate the CP violating nature of these textures analytically. For example, for texture B_2 with $\delta = 0^\circ$ (CP conserving scenario), we obtain R_ν to the first order in s_{13} using Eq. (15) and values of mass ratios given in Table 3

$$R_\nu \approx \frac{2c_{23}}{c_{12}s_{12}s_{23}\left(c_{23}^2 - s_{23}^2\right)}s_{13} - \frac{2c_{23}s_{23}}{c_{12}s_{12}\left(c_{23}^2 - s_{23}^2\right)}s_{13}.$$

Using the best-fit values given in Table 5, $|R_\nu| \approx 1.7$ which is outside 3σ range, thus, $\delta = 0^\circ$ is disallowed implying B_2 texture is necessarily CP violating. Similarly, for texture B_4, taking $\delta = 0^\circ$ R_ν can, approximately, be written as

$$R_\nu \approx \frac{s_{23}^5\left(2c_{23}^4c_{12}^2 - 2c_{12}^2s_{23}^2c_{23}^2 + 2c_{23}^2s_{12}^2 - s_{23}^2\right)}{c_{12}c_{23}^5s_{12}\left(s_{23}^4 - c_{23}^4\right)}s_{13},$$

which again result in $|R_\nu| > 1$ for best-fit values of the mixing angles. Similar analysis can be done for CP-violating textures of class C and D discussed in the following sections.

We have, also, obtained the implication of the model for neutrinoless double beta ($0\nu\beta\beta$) decay amplitude $|M_{ee}|$. It is evident from Fig. 2 that there exist a lower bound on $|M_{ee}|$ in both the textures. For texture B_2 (B_4), $|M_{ee}| < 0.03$ eV (0.06 eV). The prediction for $|M_{ee}|$ has, also, been tabulated in Table 7.

3.3 Class C

For texture C_2, the mass ratios $|R_{12}|$ and $|R_{13}|$ are equal to 1 resulting in degenerate neutrino masses which is in contradiction with neutrino oscillation data. Therefore, texture C_2 is disallowed. For textures C_1, the mass ratios $|R_{12}|$ and $|R_{13}|$, up-to first order in s_{13}, are given by

$$|R_{12}| \equiv \frac{m_1}{m_2} \approx 1 - \frac{c_{23}s_{13}\cos\delta}{c_{12}s_{12}s_{23}^3}, \tag{26}$$

$$|R_{13}| \equiv \frac{m_1}{m_3} \approx \frac{c_{23}^2}{s_{23}^2} - \frac{c_{12}c_{23}^3 s_{13}\cos\delta}{s_{12}s_{23}^5}. \tag{27}$$

It can be seen from Eq. (26) that δ should lie in first and fourth quadrant to have $|R_{12}| \equiv \frac{m_1}{m_2} < 1$. Also, for θ_{23} above maximality ($\theta_{23} > 45°$) and $\cos\delta$ positive the model predicts normal hierarchical neutrino masses. The above observations are, also, supplemented by Fig. 3. Similar analysis can, also, be done for texture C_3. In fact, it is evident from Fig. 3 that C_3 admit inverted hierarchical neutrino masses. Also, it is to be noted that the phenomenology of both the textures are found to be similar under LMA and LMA-D solutions. In Fig. 3, we have shown the allowed parameter space considering LMA solution. The Majorana phases are sharply correlated and constrained to very narrow ranges giving a lower bound on $0\nu\beta\beta$ decay amplitude $|M_{ee}|$. For texture C_1 (C_3) $|M_{ee}| >$ 0.02 (0.06) eV (Table 7). The Dirac-type CP violating phase δ is sharply constrained around 90° and 270°, thus, allowing a maximal CP violation. The Jarlskog rephasing invariant J_{CP} is non-zero which is, also, shown in Fig. 3.

3.4 Class D

For textures D_1, the mass ratios, up-to first order in s_{13}, are given by

$$|R_{12}| \equiv \frac{m_1}{m_2} \approx \frac{s_{12}^2}{c_{12}^2} + \frac{s_{12}s_{23}s_{13}\cos\delta}{c_{12}^3 c_{23}}, \tag{28}$$

$$|R_{13}| \equiv \frac{m_1}{m_3} \approx \frac{\tan\theta_{12}}{\tan\theta_{23}} s_{13}. \tag{29}$$

For texture D_1, LMA-D solution is disallowed as $|R_{12}| >$ 1 (Eq. (28)). However, for LMA solution, it is evident that $|R_{13}| < 1$ (Eq. (29)) implying normal hierarchical neutrino masses. The above analytical observations are, also, supplemented by the correlation plots in Figs. 4 and 5. In addition, the Majorana phases are sharply constrained and correlated in such a way giving vanishing value of $0\nu\beta\beta$ decay amplitude $|M_{ee}|$ (Table 7).

Texture D_2 is found to be consistent with both LMA and LMA-D descriptions with normal hierarchical neutrino masses, as shown in Figs. 6 and 7. It is evident from ($\theta_{23} - |M_{ee}|$) correlation plot in Fig. 7 that there exist a 3σ lower bound on $0\nu\beta\beta$ decay amplitude $|M_{ee}| > 0.02$ eV (see Table 7). Furthermore, in contrast to D_1, texture D_2 is found to be necessarily CP violating as depicted in (θ_{13}-J_{CP}) (Fig. 7) and (θ_{23}-δ) (Fig. 8) correlation plots.

3.5 Class E

The mass ratios for texture E_1 can be obtained from Eqs. (28) and (29) by using the transformation $c_{23} \to s_{23}$; $s_{23} \to c_{23}$ *viz.*,

$$|R_{12}| \equiv \frac{m_1}{m_2} \approx \frac{s_{12}^2}{c_{12}^2} + \frac{s_{12}c_{23}s_{13}\cos\delta}{c_{12}^3 s_{23}}, \tag{30}$$

$$|R_{13}| \equiv \frac{m_1}{m_3} \approx \tan\theta_{12}\tan\theta_{23}s_{13}. \tag{31}$$

It can be seen from Eq. (30) that E_1 is not consistent with LMA-D solution as $|R_{12}| > 1$. The allowed parameter space for LMA with NH is shown in Figs. 9 and 10. Also, the Majorana phases are correlated in such a way that $0\nu\beta\beta$ decay amplitude $|M_{ee}|$ is found to be vanishing in this case. Furthermore, the texture allows for both CP conserving and violating solutions as is evident from Fig. 10.

4 Symmetry realization

In this section, we discuss the minimal realization of two-zero texture of M_ν^{-1}. Motivated by the pivotal character played by the discrete flavor symmetry groups in explaining the observed neutrino oscillation data [37,38], we obtain the A_4 flavor group based symmetry realisation of inverse neutrino mass matrix (M_ν^{-1}) by extending the standard model particle content in the lepton sector. A_4 is a non-Abelian discrete group of even permutations. A_4 group is a orientation-preserving symmetry of a regular tetrahedron. It has four irreducible representations 1, $1'$, $1''$ and 3 and can be generated using S and T generators satisfying the relations

$$S^2 = T^3 = (ST)^3 = 1.$$

Here, we choose basis for A_4 group in which T generator takes the diagonal form. The reason behind choosing this particular representation is that it facilitates the diagonal mass matrix for charged leptons. In T-diagonal basis, one dimensional unitary representation 1, $1'$ and $1''$ with generator S and T can be written as

$$1: \quad S = 1, \quad T = 1,$$
$$1': \quad S = 1, \quad T = \omega,$$
$$1'': \quad S = 1, \quad T = \omega^2,$$

such that $\omega = e^{i2\pi/3}$ whereas three-dimensional unitary representation is given by

$$T = \begin{pmatrix} 1 & 0 & 0 \\ 0 & \omega & 0 \\ 0 & 0 & \omega^2 \end{pmatrix}, \quad S = \frac{1}{3}\begin{pmatrix} -1 & 2 & 2 \\ 2 & -1 & 2 \\ 2 & 2 & -1 \end{pmatrix}.$$

The multiplication rules for the representations of A_4 are as follows

$$1' \otimes 1' = 1'', \quad 1'' \otimes 1'' = 1',$$
$$1' \otimes 1'' = 1, \quad 1'' \otimes 1 = 1'',$$
$$1 \otimes 1' = 1', \quad 3 \otimes 1' = 3, \quad 3 \otimes 1'' = 3,$$

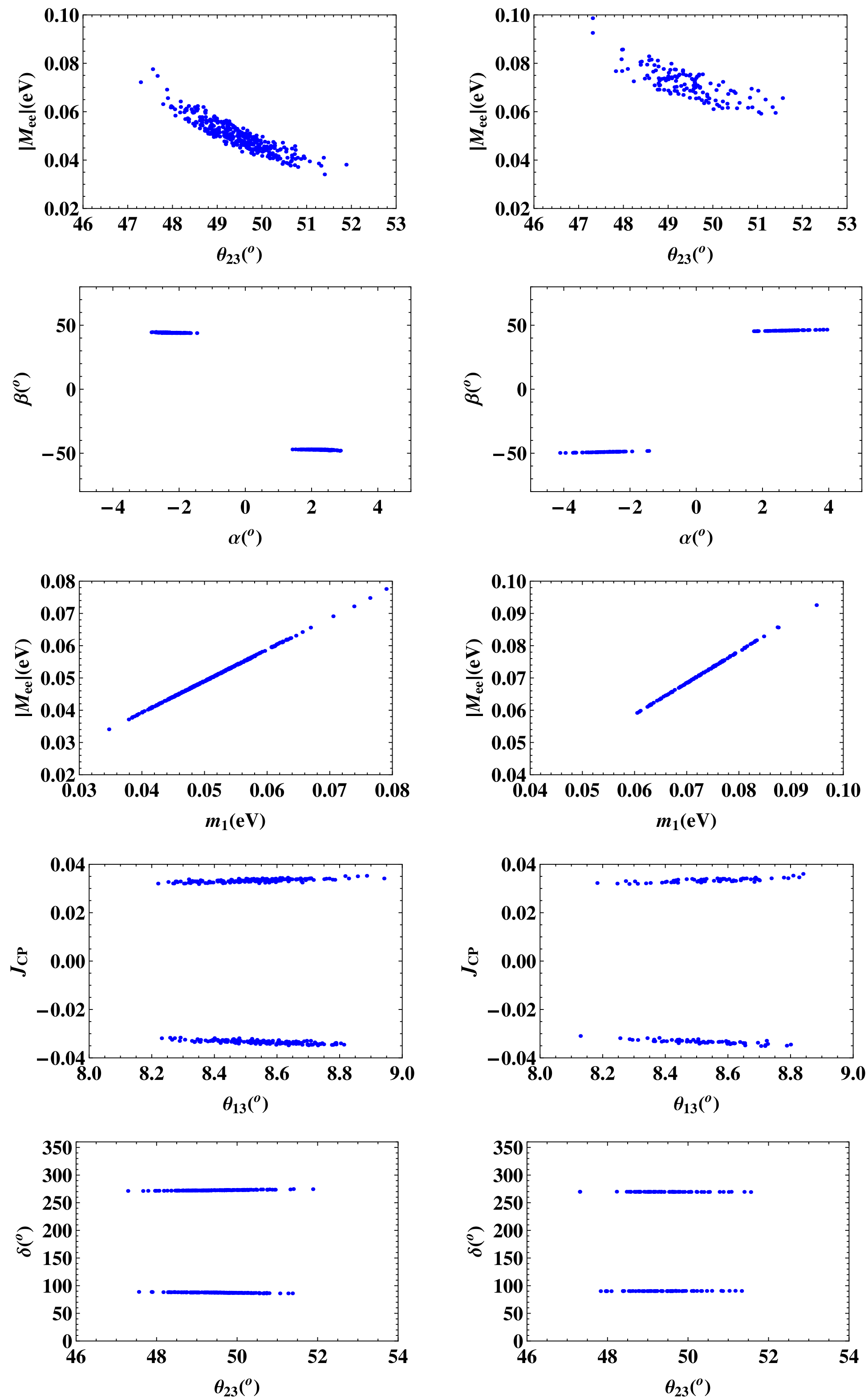

Fig. 3 Correlation plots for textures C_1-NH (left panel) and C_3-IH (right panel) under LMA scenario

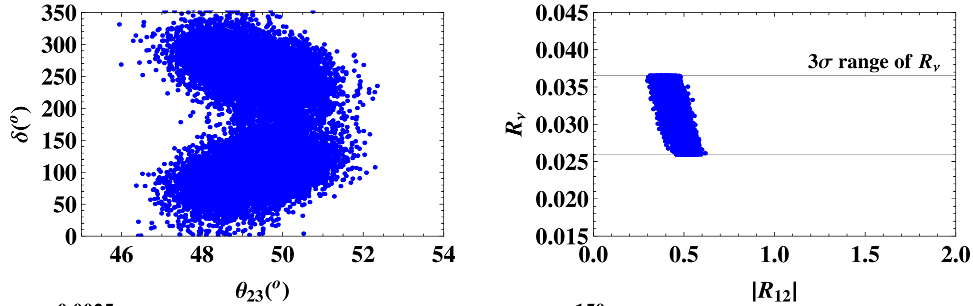

Fig. 4 Correlation plots between $(\theta_{23} - \delta)$ (left) and $(|R_{12}| - R_\nu)$ (right) for D_1 texture under LMA solution with NH

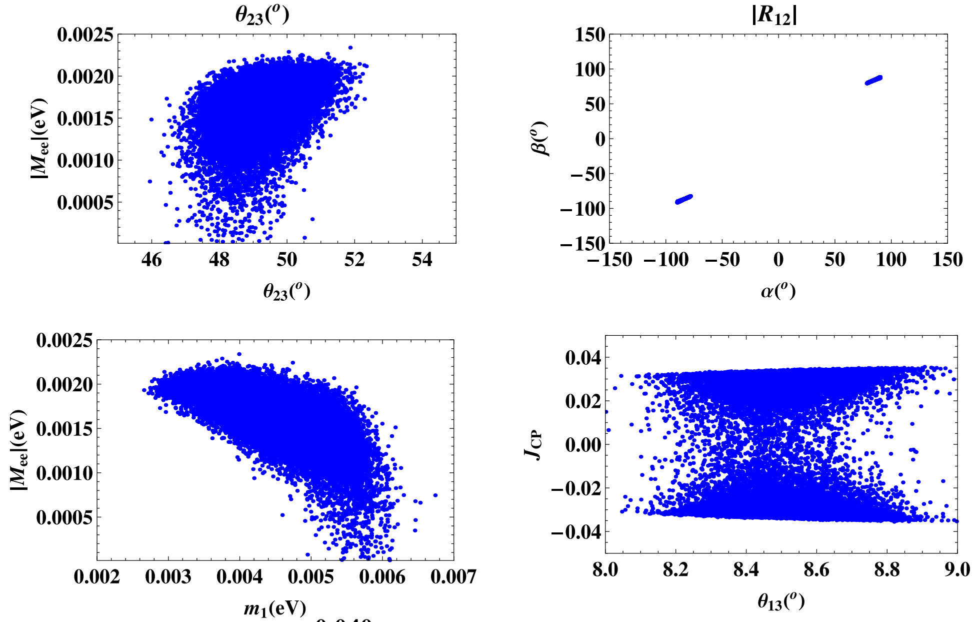

Fig. 5 Correlation plots for D_1 texture under LMA solution with NH

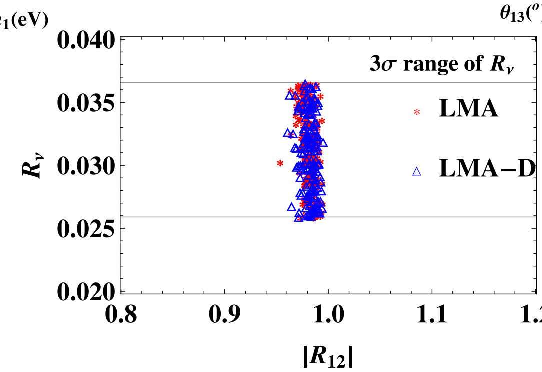

Fig. 6 Correlation between $(|R_{12}| - R_\nu)$ for D_2 texture

$$3 \otimes 3 = 1 \oplus 1' \oplus 1'' \oplus 3_s \oplus 3_a.$$

In the T-diagonal basis, the Clebsch–Gordan decomposition of two triplets, a = (a_1, a_2, a_3) and b = (b_1, b_2, b_3) is given as

$$\begin{aligned}
(a \otimes b)_1 &= a_1 b_1 + a_2 b_3 + a_3 b_2, \\
(a \otimes b)_{1'} &= a_3 b_3 + a_1 b_2 + a_2 b_1, \\
(a \otimes b)_{1''} &= a_2 b_2 + a_1 b_3 + a_3 b_1, \\
(a \otimes b)_{3_s} &= \frac{1}{3}\,(2a_1 b_1 - a_2 b_3 - a_3 b_2, 2a_3 b_3 - a_1 b_2 \\
&\quad - a_2 b_1, 2a_2 b_2 - a_1 b_3 - a_3 b_1)\,, \\
(a \otimes b)_{3_a} &= \frac{1}{2}\,(a_2 b_3 - a_3 b_2, a_1 b_2 - a_2 b_1, a_1 b_3 - a_3 b_1)\,.
\end{aligned} \tag{32}$$

Here, we have worked in the framework of Type-I seesaw. In addition, we have minimally extended the standard model by adding three right-handed neutrino fields ($\nu_{iR}; i = 1, 2, 3$) and one scalar field (χ), having singlet representation under A_4 symmetry as shown in the Table 8. In general, for any Yukawa coupling to be non-zero, its Yukawa Lagrangian term must be in singlet-invariant representation of A_4 with mass dimension four at tree level.

Texture B_4:

Using the tensor products in Eq. (32), the invariant Yukawa Lagrangian is given by

$$\begin{aligned}
-\mathcal{L} &= \ldots\ldots + y_e \bar{D}_{eL}\phi e_R + y_\mu \bar{D}_{\mu L}\phi \mu_R + y_\tau \bar{D}_{\tau L}\phi \tau_R \\
&+ y_1 \bar{D}_{eL}\tilde{\phi}\nu_{eR} + y_2 \bar{D}_{\mu L}\tilde{\phi}\nu_{\mu R} + y_3 \bar{D}_{\tau L}\tilde{\phi}\nu_{\mu R} \\
&+ \frac{1}{2}\left[M_1(\nu_{1R}^T C^{-1}\nu_{1R}) + M_2(\nu_{2R}^T C^{-1}\nu_{3R} + \nu_{3R}^T C^{-1}\nu_{2R})\right]
\end{aligned}$$

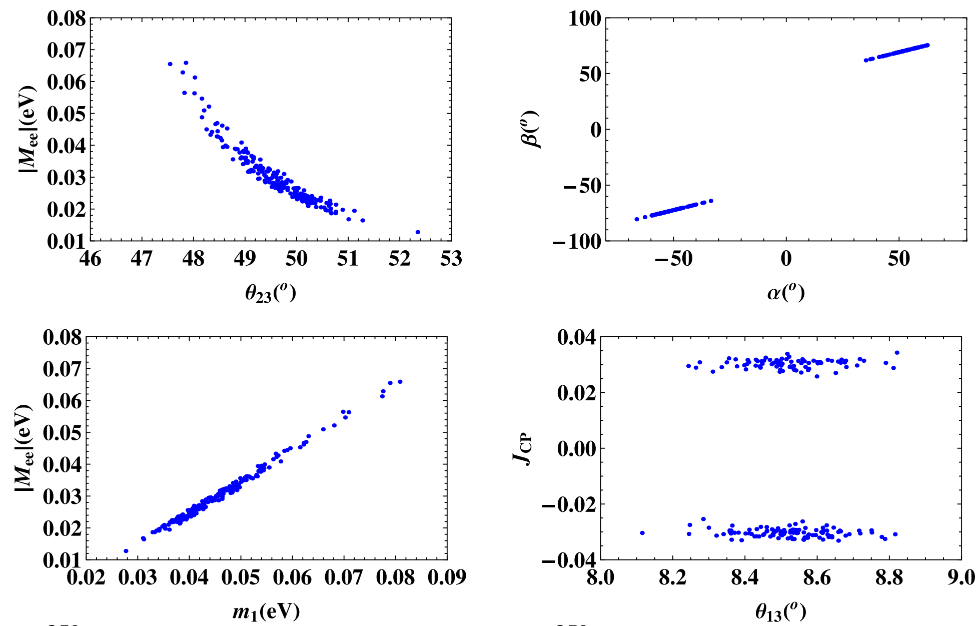

Fig. 7 Correlation plots for D_2 texture under LMA solution with NH

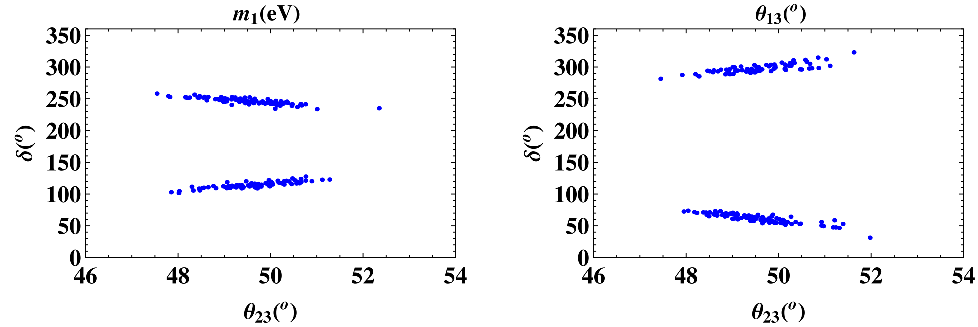

Fig. 8 Correlation between $(\theta_{23} - \delta)$ for D_2 texture with NH under LMA (left) and LMA-D (right)

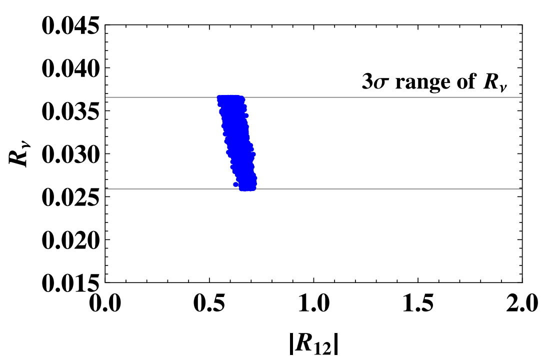

Fig. 9 Correlation between $(|R_{12}| - R_\nu)$ for texture E_1 under LMA solution with NH

$$+\frac{1}{2}\left[\left(y_{\chi 1}(\nu_{2R}^T C^{-1}\nu_{2R}) + y_{\chi 2}(\nu_{1R}^T C^{-1}\nu_{3R} + \nu_{3R}^T C^{-1}\nu_{1R})\right)\chi\right], \tag{33}$$

where y_k, y_i ($k = e, \mu, \tau$; $i = 1, 2, 3$) are Yukawa coupling constants, $M_{1,2}$ are bare mass terms for right-handed Majorana neutrinos, $y_{\chi 1,2}$ denotes Yukawa coupling constant for interaction terms with scalar field χ and $\tilde{\phi} = i\tau_2\phi^*$; τ_2 being Pauli matrix.

The dots in the Lagrangian represents the other kinetic and scalar potential terms. We have restricted up to Yukawa interactions pertaining to mass terms. Spontaneous symmetry breaking (SSB) occurred with vacuum expectation values (vev's) v and w for the Higgs doublet and scalar singlet field, respectively. The Yukawa Lagrangian (Eq. (33)) leads to the mass matrices as

$$M_l = \begin{pmatrix} y_e v & 0 & 0 \\ 0 & y_\mu v & 0 \\ 0 & 0 & y_\tau v \end{pmatrix}, \quad M_D = \begin{pmatrix} y_1 v & 0 & 0 \\ 0 & y_2 v & 0 \\ 0 & 0 & y_3 v \end{pmatrix} \tag{34}$$

and

$$M_R = \begin{pmatrix} M_1 & 0 & y_{\chi 2} w \\ 0 & y_{\chi 1} w & M_2 \\ y_{\chi 2} w & M_2 & 0 \end{pmatrix}, \tag{35}$$

where M_l, M_D and M_R corresponds to charged lepton mass matrix, Dirac mass matrix and right-handed Majorana mass matrix, respectively (Table 8).

Type-I seesaw contribution to effective Majorana neutrino mass matrix is given by

$$M_\nu = M_D M_R^{-1} M_D^T. \tag{36}$$

Also, the inverse neutrino mass matrix can be written as

$$M_\nu^{-1} = M_D^{-T} M_R M_D^{-1}. \tag{37}$$

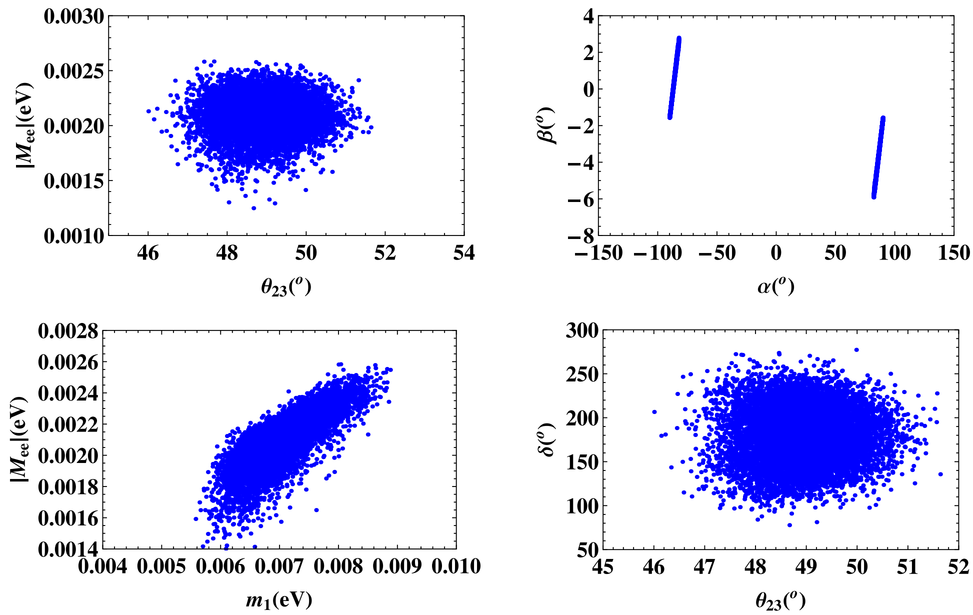

Fig. 10 Correlation plots for texture E_1 under LMA solution with NH

Table 8 Field content and charge assignments in the model under $SU(2)_L$ and A_4 symmetries

Symmetry	D_{eL}	$D_{\mu L}$	$D_{\tau L}$	e_R	μ_R	τ_R	ν_{1R}	ν_{2R}	ν_{3R}	ϕ	χ	Obtained two-zero textures
$SU(2)_L$	2	2	2	1	1	1	1	1	1	2	1	
A_4	1	$1''$	$1'$	1	$1'$	$1''$	1	$1'$	$1''$	1	$1'$	$B_4=\begin{pmatrix} X & 0 & X \\ 0 & X & X \\ X & X & 0 \end{pmatrix}$
	1	$1''$	$1'$	1	$1'$	$1''$	1	$1'$	$1''$	1	$1''$	$C_1=\begin{pmatrix} X & X & 0 \\ X & 0 & X \\ 0 & X & X \end{pmatrix}$

In M_D-diagonal basis, the peculiar feature of implementation of type-I seesaw for M_ν^{-1} is that the zero(s) in M_R corresponds to zero(s) in M_ν^{-1}. Using the Eqs. (34) and (35), the M_ν^{-1} is given by

$$M_\nu^{-1} = \begin{pmatrix} \frac{M_1}{v^2 y_1^2} & 0 & \frac{y_{\chi_1} w}{v^2 y_1 y_3} \\ 0 & \frac{y_{\chi_2} w}{v^2 y_3^2} & \frac{M_2}{v^2 y_2 y_3} \\ \frac{y_{\chi_1} w}{v^2 y_1 y_3} & \frac{M_2}{v^2 y_2 y_3} & 0 \end{pmatrix}, \tag{38}$$

which symbolically can be written as

$$M_\nu^{-1} = \begin{pmatrix} X & 0 & X \\ 0 & X & X \\ X & X & 0 \end{pmatrix} \tag{39}$$

corresponding to texture B_4.

Texture C_1:

For the realization of texture C_1, we change the irreducible representation of scalar field χ to be $1''$. The relevant Yukawa Lagrangian is

$$\begin{aligned} -\mathcal{L} = \ldots\ldots + y_e \bar{D}_{eL}\phi e_R + y_\mu \bar{D}_{\mu L}\phi \mu_R + y_\tau \bar{D}_{\tau L}\phi \tau_R \\ + y_1 \bar{D}_{eL}\tilde{\phi}\nu_{eR} + y_2 \bar{D}_{\mu L}\tilde{\phi}\nu_{\mu R} + y_3 \bar{D}_{\tau L}\tilde{\phi}\nu_{\mu R} \\ + \frac{1}{2}\Big[M_1(\nu_{1R}^T C^{-1}\nu_{1R}) + M_2(\nu_{2R}^T C^{-1}\nu_{3R} \\ + \nu_{3R}^T C^{-1}\nu_{2R})\Big] \\ + \frac{1}{2}\Big[\Big(y_{\chi_1}(\nu_{3R}^T C^{-1}\nu_{3R}) + y_{\chi_2}(\nu_{1R}^T C^{-1}\nu_{2R} \\ + \nu_{2R}^T C^{-1}\nu_{1R})\Big)\chi\Big] \end{aligned} \tag{40}$$

where $y_k, y_i (k = e, \mu, \tau; i = 1, 2, 3)$ are Yukawa coupling constants, $M_{1,2}$ are bare mass terms for right-handed Majorana neutrinos, $y_{\chi_{1,2}}$ denotes Yukawa coupling constant for interaction terms with scalar field χ and $\tilde{\phi} = i\tau_2\phi^*$; τ_2 being Pauli matrix.

After SSB, charged lepton mass matrix and Dirac mass matrix remains diagonal as shown in Eq. (34). But Majorana mass matrix gets modified and takes the form

$$M_R = \begin{pmatrix} M_1 & y_{\chi_2} w & 0 \\ y_{\chi_2} w & 0 & M_2 \\ 0 & M_2 & y_{\chi_1} w \end{pmatrix}. \tag{41}$$

In M_D-diagonal basis, the inverse neutrino mass matrix is given by

$$M_\nu^{-1} = \begin{pmatrix} \frac{M_1}{v^2 y_1^2} & \frac{y_{\chi_2} w}{v^2 y_1 y_2} & 0 \\ \frac{y_{\chi_2} w}{v^2 y_1 y_2} & 0 & \frac{M_2}{v^2 y_2 y_3} \\ 0 & \frac{M_2}{v^2 y_2 y_3} & \frac{y_{\chi_1} w}{v^2 y_3^2} \end{pmatrix}, \tag{42}$$

which symbolically can be written as

$$M_\nu^{-1} = \begin{pmatrix} X & X & 0 \\ X & 0 & X \\ 0 & X & X \end{pmatrix}, \tag{43}$$

corresponding to texture C_1.

5 Conclusions

In conclusion, we have investigated the phenomenological implications of two-zero textures in inverse neutrino mass matrix M_ν^{-1}. In the basis where Dirac neutrino mass matrix M_D is diagonal, zeros in right-handed Majorana neutrino mass matrix M_R corresponds to zeros of M_ν^{-1}. We have, also, proposed symmetry realization, based on discrete flavor group A_4, wherein such texture zeros can emerge in M_ν^{-1}. Further, we investigate the viability of all two-zero textures in M_ν^{-1} under LMA and LMA-D solutions. We have categorized the possible textures in five classes *viz.* class A, B, C, D and E. Out of fifteen possible two-zero textures of M_ν^{-1}, seven are found to be in consonance with LMA and/or LMA-D scenario. The general remarks about the obtained phenomenology are as under:

- The textures in class A are all disallowed as they do not reproduce the correct neutrino phenomenology. Thus, texture with $\left(M_\nu^{-1}\right)_{11} = 0$ is disallowed, in general.
- In class B, B_2 and B_4 textures are consistent with both LMA and LMA-D solutions. B_2 (B_4) predicts normal (inverted) hierarchical neutrino masses. For texture B_2, the 3σ lower bound on $0\nu\beta\beta$ decay amplitude $|M_{ee}|$ is found to be 0.02 eV (0.04 eV) under LMA and LMA-D, respectively. For B_4 texture, it is about 0.06 eV for both LMA and LMA-D solutions.
- In class C, C_2 is disallowed. C_1 and C_3 textures are consistent with both LMA and LMA-D solutions. C_1 (C_3) predicts normal (inverted) hierarchical neutrino masses. For texture C_1 (C_3), the 3σ lower bound on $|M_{ee}|$ is 0.02 eV (0.06) eV under both LMA and LMA-D solutions.
- For textures B_2, B_4, C_1 and C_3, the Dirac and Majorana-type CP violating phases are sharply constrained and these textures are found to be necessarily CP violating.
- Textures D_1 and E_1 predict normal hierarchical neutrino masses and are found to be consistent with LMA solution. LMA-D solution is disallowed by these textures. Also, $|M_{ee}|$ is vanishing in these textures. In general, we conclude that the textures for which LMA-D is disallowed, $|M_{ee}|$ is vanishing. Similar inference is observed in Ref. [11] wherein the authors analyzed phenomenology of Majorana neutrino textures in the light of LMA-D solution.
- Texture D_2 predicts normal hierarchical neutrino masses and is consistent with both LMA and LMA-D phenomenology. In LMA (LMA-D) scenario, there exist a 3σ lower bound on $|M_{ee}| > 0.01$ eV (0.02 eV).
- The generic feature of the class of model, discussed in the present work, is the existence of neutrino mass hierarchy degeneracy in a particular texture. For example, if a texture is allowed by LMA solution with "X" neutrino mass hierarchy then, if LMA-D is allowed, it is allowed with the same hierarchy "X".

The allowed two-zero texture of M_ν^{-1} *viz.* B_2, B_4, C_1, C_3, D_1, D_2 and E_1 has imperative predictions for $|M_{ee}|$ [33]. Except for D_1 and E_1 textures, the predicted 3σ lower bound on $0\nu\beta\beta$ decay amplitude $|M_{ee}|$ is $\mathcal{O}(10^{-2})$ which is within the sensitivity reach of $0\nu\beta\beta$ decay experiments like SuperNEMO [39], KamLAND-Zen [40], NEXT [41,42], and nEXO [43]. For example, the non-observation of $0\nu\beta\beta$ decay down to these high sensitivities will refute all the textures except D_1 and E_1. Also, we have shown that the allowed M_ν^{-1} textures can be accommodated in an extension of the SM with three right-handed neutrinos and one scalar singlet field. As representative realizations, we have obtained two such textures B_4 and C_1 within Type-I seesaw scenario using A_4 discrete flavor symmetry.

Acknowledgements M. K. acknowledges the financial support provided by Department of Science and Technology (DST), Government of India vide Grant no. DST/INSPIRE Fellowship/2018/IF180327. The authors, also, acknowledge Department of Physics and Astronomical Science for providing necessary facility to carry out this work.

Data Availability Statement This manuscript has no associated data or the data will not be deposited. [Authors' comment: The present study is a phenomenological investigation and has no additional associated data from any repository.]

Funded by SCOAP^3. SCOAP^3 supports the goals of the International Year of Basic Sciences for Sustainable Development.

References

1. S.T. Petcov, M. Piai, Phys. Lett. B **533**, 94–106 (2002)
2. L. Wolfenstein, Phys. Rev. D **17**, 2369–2374 (1978)
3. P.S. Bhupal Dev et al., SciPost Phys. Proc. **2**, 001 (2019)
4. C. Biggio, M. Blennow, E. Fernandez-Martinez, JHEP **08**, 090 (2009)
5. P. Coloma et al., JHEP **04**, 116 (2017)
6. P.B. Denton, Y. Farzan, I.M. Shoemaker, JHEP **07**, 037 (2018)
7. P.B. Denton, J. Gehrlein, arXiv:2204.09060 [hep-ph]
8. I. Esteban et al., JHEP **08**, 180 (2018)
9. P. Minkowski, Phys. Lett. B **67**, 421–428 (1977)
10. R.N. Mohapatra, G. Senjanovic, Phys. Rev. D **23**, 165 (1981)
11. H. Borgohain, D. Borah, J. Phys. G **47**(12), 125002 (2020)
12. M. Ghosh, S. Goswami, A. Mukherjee, Nucl. Phys. B **969**, 115460 (2021)
13. Z.H. Zhao, X. Zhang, S.S. Jiang, C.X. Yue, Int. J. Mod. Phys. A **35**(07), 2050039 (2020)
14. K. N. Deepthi, S. Goswami, K. N. Vishnudath, T. K. Poddar, Phys. Rev. D **102**(01), 015020 (2020)
15. D. Borah, M. Ghosh, S. Gupta, S.K. Raut, Phys. Rev. D **96**(5), 055017 (2017)
16. E.I. Lashin, N. Chamoun, Phys. Rev. D **85**, 113011 (2012)
17. H. Fritzsch, Z.Z. Xing, Nucl. Phys. B **556**, 49–75 (1999). https://doi.org/10.1016/S0550-3213(99)00337-5
18. A. Merle, W. Rodejohann, Phys. Rev. D **73**, 073012 (2006)
19. S. Dev, S. Kumar, Mod. Phys. Lett. A **22**, 1401–1410 (2007)
20. H. Fritzsch, Z.Z. Xing, S. Zhou, JHEP **09**, 083 (2011)
21. P.H. Frampton, S.L. Glashow, D. Marfatia, Phys. Lett. B **536**, 79–82 (2002)
22. B.R. Desai, D.P. Roy, A.R. Vaucher, Mod. Phys. Lett. A **18**, 1355–1366 (2003)
23. Z.Z. Xing, Phys. Lett. B **530**, 159–166 (2002)
24. W.L. Guo, Z.Z. Xing, Phys. Rev. D **67**, 053002 (2003)
25. M. Singh, G. Ahuja, M. Gupta, PTEP **2016**(12), 123B08 (2016)
26. L. Lavoura, Phys. Lett. B **609**, 317–322 (2005)
27. S. Verma, Nucl. Phys. B **854**, 340–349 (2012)
28. S. Choubey, D. Pramanik, JHEP **12**, 133 (2020)
29. P.A. Zyla et al. [Particle Data Group], PTEP **2020**(08), 083C01 (2020)
30. P.I. Krastev, S.T. Petcov, Phys. Lett. B **205**, 84–92 (1988)
31. C. Jarlskog, Phys. Rev. Lett. **55**, 1039 (1985)
32. O.G. Miranda, M.A. Tortola, J.W.F. Valle, A.I.P. Conf, Proc. **917**(01), 100–107 (2007)
33. K.N. Vishnudath, S. Choubey, S. Goswami, Phys. Rev. D **99**(09), 095038 (2019)
34. F.J. Escrihuela, O.G. Miranda, M.A. Tortola, J.W.F. Valle, Phys. Rev. D **80**, 105009 (2009)
35. Y. Farzan, M. Tortola, Front. Phys. **6**, 10 (2018)
36. P.F. de Salas et al., JHEP **02**, 071 (2021)
37. H. Ishimori et al., Lect. Notes Phys. **858**, 1–227 (2012)
38. E. Ma, G. Rajasekaran, Phys. Rev. D **64**, 113012 (2001)
39. A.S. Barabash, J. Phys: Conf. Ser. **375**, 042012 (2012)
40. A. Gando et al., Phys. Rev. Lett. **117**, 082503 (2016)
41. F. Granena et al., arXiv:0907.4054 [hep-ex]
42. J.J. Gomez-Cadenas et al., Adv. High Energy Phys. **2014**, 907067 (2014)
43. C. Licciardi, J. Phys. Conf. Ser. **888**, 012237 (2017)